Geophysical Research Letters

RESEARCH LETTER
10.1029/2020GL087405

Structural Variability Within the Kane Oceanic Core Complex From Full Waveform Inversion and Reverse Time Migration of Streamer Data

Min Xu[1,2,3], **Xu Zhao**[1,2,3,4], **and J. Pablo Canales**[5]

[1]CAS Key Laboratory of Ocean and Marginal Sea Geology, South China Sea Institute of Oceanology, Guangzhou, China, [2]Innovation Academy of South China Sea Ecology and Environmental Engineering, Chinese Academy of Sciences, Guangzhou, China, [3]Southern Marine Science and Engineering Guangdong Laboratory, Guangzhou, China, [4]College of Earth and Planetary Sciences, University of Chinese Academy of Sciences, Beijing, China, [5]Department of Geology and Geophysics, Woods Hole Oceanographic Institution, Woods Hole, MA, USA

Abstract The origin and distribution of the gabbroic bodies provide crucial information to understand the formation and evolution processes of the oceanic core complexes (OCCs). Nevertheless, images of the shape of the gabbroic bodies across the domes and gabbroic intrusion into the mantle have remained elusive. High-resolution acoustic early-arrival full waveform inversion tomography models obtained along and across the Kane OCC characterize the detailed lateral variability in structure and composition of the upper ~2 km of this well-developed OCC. Reverse time migration images show the gabbroic plutons embedded in mantle rocks are seismically transparent, while more reflective sections correspond to the layered magmatic crust. Lithological interpretation shows heterogeneous distribution of gabbroic bodies within the Kane OCC, indicating strong spatial and temporal variability in magmatism during fault exhumation. Our results will also be of high value for future scientific ocean drilling efforts in the area.

Plain Language Summary The complex array of magmatic and tectonic processes, both of which vary spatially and through time, gives rise to a heterogeneous lithospheric section at mid-ocean ridges. At slow-spreading ridges, tectonic extension can be accommodated by long-lived (e.g., 1–2 Ma) oceanic detachment, exhuming deep crustal and upper mantle lithologies to form oceanic core complexes (OCCs). The Kane OCC, located ~30–55 km off-axis the Mid-Atlantic Ridge between ~23°20′N and ~23°40′N, was formed by a long-lived detachment fault between ~3.3 and 2.1 Ma under conditions of strongly asymmetrical spreading. The lithospheric structure of the Kane OCC is compositionally and structurally heterogeneous and far from the standard ophiolite-based Penrose model which typically represents oceanic lithosphere formed along the fast-spreading ridges. Understanding the origin and distribution of the gabbroic bodies is crucial to understand the magmatic activity during the formation and evolution processes of Kane OCC. Here we present advanced seismic imaging techniques to map the structural variability within the Kane OCC from full waveform inversion and reverse time migration of long streamer seismic data. Our results show the detailed shape of the gabbroic bodies, and the heterogeneous distribution of gabbroic bodies within the Kane OCC indicates strong spatial and temporal variability in magmatism.

Key Points:
- Full waveform inversion and reverse time migration are applied to long offset streamer seismic data acquired at Kane oceanic core complex
- High-resolution velocity models and migration images of the upper lithosphere shows structural variability beneath most of the main domes
- The heterogeneous distribution of gabbroic bodies indicates strong spatial and temporal variability in magmatism during fault exhumation

Supporting Information:
- Supporting Information S1

Correspondence to:
M. Xu,
mxu@scsio.ac.cn

Citation:
Xu, M., Zhao, X., & Canales, J. P. (2020). Structural variability within the Kane oceanic core complex from full waveform inversion and reverse time migration of streamer data. *Geophysical Research Letters*, *46*, e2020GL087405 https://doi.org/10.1029/2020GL087405

Received 5 FEB 2020
Accepted 19 MAR 2020
Accepted article online 28 MAR 2020

1. Introduction

Oceanic detachment faults (ODFs) on the flanks of mid-ocean ridges exhume lower crustal and mantle rocks to the seafloor, forming oceanic core complexes (OCCs) (e.g., Cann et al., 1997; Escartín et al., 2003; Tucholke et al., 1998). Although numerical simulations predict that long-lived detachment faulting is favored during periods of reduced magma supply (Buck et al., 2005; Tucholke et al., 2008), seafloor observations and drilling indicate that gabbroic rocks are, in many cases, a large component of the lithological substrate of the oceanic detachment's footwall (e.g., Blackman et al., 2011; Dick et al., 2000, 2008; Ildefonse et al., 2007). This apparent paradox could be explained if magma intrusion during detachment faulting is accommodated in the ductile asthenosphere, thus allowing OCC formation under high magma intrusion rates (Olive et al., 2010). Therefore, the spatial distribution and size of gabbroic rocks as well as that of ultramafic lithologies beneath OCCs is of fundamental importance for understanding their formation and evolution and for testing the validity of current conceptual models (e.g., Escartín & Canales, 2011; Ildefonse et al., 2007; MacLeod et al., 2009).

Detailed seafloor observations at a few OCCs by dredging and/or submersibles reveal that major lithologies such as basalts, gabbros, and serpentinized peridotites can vary across the surface of an OCC at lateral scales of ~10 km as well as at smaller lateral scales of only a few hundred meters (e.g., Blackman et al., 2002; Dick et al., 2019, 2008; Escartín et al., 2017). Geophysical methods such as traveltime seismic tomography have been used to infer the large-scale lithological distribution beneath the seafloor within the upper ~1.5 km of the exhumed lithosphere (Canales et al., 2008; Dannowski et al., 2010; J. L. Harding et al., 2017; Henig et al., 2012; Planert et al., 2010; Xu et al., 2009), showing excellent agreement with large-scale seafloor geology and drilling results (Canales et al., 2008; Henig et al., 2012; Xu et al., 2009). Efforts to geophysically image smaller-scale subseafloor lithological heterogeneities of OCCs have been very limited (Canales, 2010; Harding et al., 2016) but have shown great promise in using advanced imaging techniques such as full waveform inversion (FWI) to provide constraints on subseafloor structure at scales comparable to those of seafloor geological observations.

At Atlantis Massif on the Mid-Atlantic Ridge flank, FWI of multichannel seismic (MCS) streamer data along a ~20-km-long profile transecting the dominantly gabbroic Central Dome and the serpentinized Southern Ridge reveals the top and edges of the high-velocity, gabbroic core of the Central Dome and constrains its thickness to ~2.5 km (Harding et al., 2016). The relatively uniform gabbroic rocks drilled at the Central Dome (Blackman et al., 2011) are formed by a series of sill-like small intrusive bodies (Grimes et al., 2011), but FWI is unlikely to resolve such fine-scale structure if neighboring gabbroic sills have similar elastic properties. At the Cain Dome in the Kane OCC, FWI of MCS streamer data along two intersecting profiles ~14–18 km in length shows that the gabbroic body beneath the detachment fault in its eastern flank near the termination is ~1,000–1,350 m thick and is underlain by a ~300-m-thick layer of low-velocity material interpreted as serpentinized peridotite (Canales, 2010).

Here we present tomography and imaging results from applying time domain acoustic FWI and reverse time migration (RTM) to the MCS streamer data set collected in 2001 across the Kane OCC (see Text S1 in the supporting information). Seismic structure derived from streamer traveltime tomography has been previously published and used to infer the large-scale heterogeneity of the OCC (Canales et al., 2008; Xu et al., 2009). We use these published results as starting models for resolving the small-scale structure of the OCC along the six existing seismic profiles. We show that the basaltic layer has a maximum thickness of 1.7 km and a total estimated volume of >64 km^3 beneath the southern volcanic field, while it has a more uniform thickness of ~1.2 km beneath the northern volcanic field. The thickness of the basaltic layer in the hanging wall averages ~1.0 km. The interpreted gabbroic bodies show a bimodal distribution in terms of the size and location within the Kane OCC, with a few isolated small gabbroic bodies present within the predominantly serpentinized Abel Dome, indicating the Kane ODF was initiated under a magma-limited environment. The large gabbroic plutons intruded beneath the ODF beneath the eastern flank of the Cain and Babel Domes have a total length of ~17 km and an average thickness of ~0.6 km. The total estimated volume of these gabbroic plutons could be >80 km^3, suggesting larger and more frequent intrusions and robust magmatism during the late stage of Kane OCC formation. There are also ongoing efforts for IODP drilling at Kane OCCs, and our results are the primary geophysical data driving these efforts and they will enable broadening the interpretation of any future drill hole into its regional and global context.

2. Geological and Geophysical Context

The Kane OCC is located ~30–55 km off-axis the Mid-Atlantic Ridge between ~23°20′N and ~23°40′N immediately south of the Kane Transform Fault on the North America plate (Figure 1). It covers an area of ~23 km by ~40 km in dip and strike directions, respectively. It was formed by a long-lived detachment fault between ~3.3 and 2.1 Ma under conditions of strongly asymmetrical spreading, with a rate of 17.9 mm/a on the OCC side, and 7.9 mm/a to the east between Chrons 2 and 2A (Williams, 2007). The exposed detachment fault exhibits a set of uplifted corrugated domes (Babel, Abel, Cain, Adam, and Eve, following the nomenclature of Dick et al., 2008) that are elevated up to a kilometer or more above adjacent seafloor and is cut by two major west facing, high-angle normal faults (West and East Faults) that likely formed in response to footwall bending during exhumation (Figure 1a) (e.g., Tucholke et al., 1998). The breakaway, where the detachment fault initially nucleated, is defined by a linear, isochron-parallel ridge that marks the older limit of fault corrugations (Figure 1a). It extends continuously for more than 40 km with a small offset near 23°30′N. The

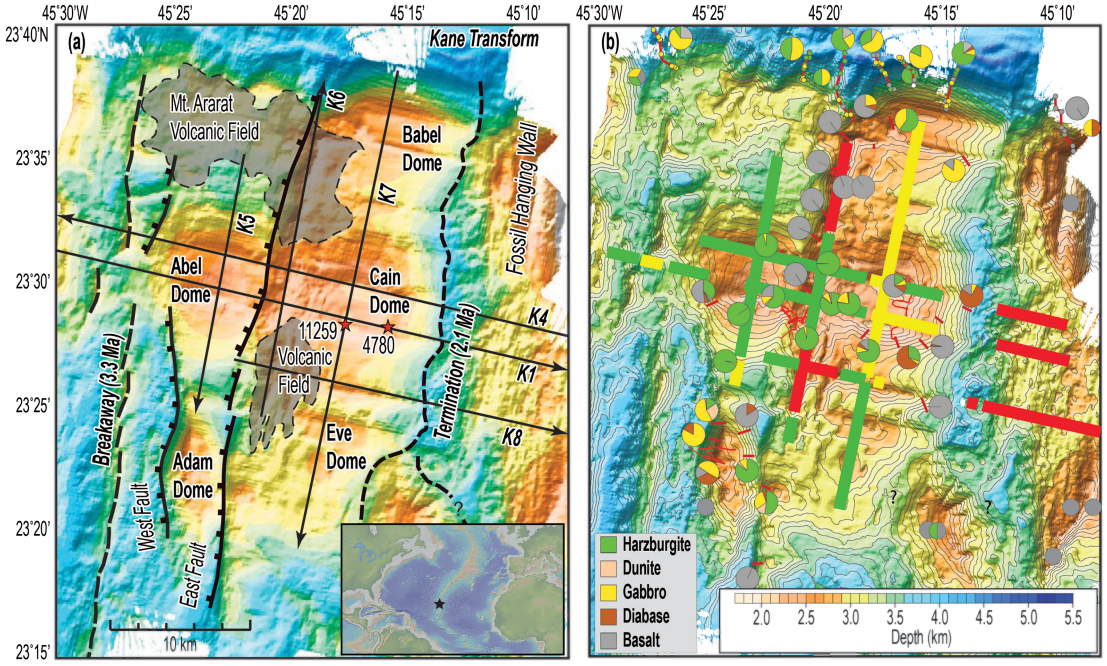

Figure 1. (a) Shaded-relief map of the Kane OCC with simplified tectonic interpretation (adapted from Dick et al., 2008). Black lines locate seismic profiles with shooting direction indicated by arrows. Red stars with shot numbers show positions of two example shot gathers displayed in Figure S1. The black star in the inset shows the study location on the MAR. (b) Interpretation of upper basement composition along the Kane MCS profiles based on TT velocity characteristics (Xu et al., 2009). Along the profiles, red presents pillow basalts (±sheeted dikes), yellow is dominantly gabbros, and green indicates serpentinized peridotites. Pie diagrams show lithological proportions by weight of samples obtained from ROV/submersible dives and dredges on two cruises: KANAUT Expedition (Auzende et al., 1994) and R/V *Knorr* Cruise 180-2 (Dick et al., 2008); inset at bottom shows the key to lithology. Dredge, Jason II, and Nautile tracks are shown in red.

termination is defined by a valley between the smooth detachment fault surface and the rougher adjacent terrain of the fossil hanging wall that marks the young limit of fault corrugations (Figure 1a). It sinuously follows corrugated domes in the detachment surface.

Extensive geological sampling on the Kane OCC has been done by dredge and ROV on *R/V Knorr* Cruise 180-2 (Dick et al., 2008) and complemented by sampling done along the southern wall of the Kane Transform Fault (northern wall of the OCC) during submersible dives of the KANAUT Expedition (Auzende et al., 1994) (Figure 1b). Details of the lithological structure of the Kane OCC are given by Dick et al. (2008). The geological sampling indicates that mantle peridotites, gabbros, and diabase dikes are exposed in the detachment footwall and in outward facing high-angle normal fault scarps and slide scars along the East Fault that cut through the detachment. The central and western parts of the Kane OCC are predominantly ultramafic, while both peridotites and gabbros are exposed along the northern edge of the OCC (e.g., Dick et al., 2008). Slide scars along the East Fault expose massive outcrops of serpentinized peridotite at the center of the OCC, providing direct evidence of the footwall composition there (Dick et al., 2008). There are two volcanic fields erupted off axis (Figure 1a), which might be related to stress distribution in the detachment fault as it was exhumed, with lower part in compression and upper part in extension as the footwall rolled over (Parnell-Turner et al., 2017). This differential stress could force any melt at depth in the footwall to erupt on the detachment surface and result in surficial volcanism along the active East Fault (Tucholke et al., 2001).

The subsurface velocity structure shows an excellent agreement with large-scale seafloor geology and drilling/diving results (Canales et al., 2008; Xu et al., 2009) (Figure 1b). Areas with low uppermost velocities near the seafloor (<3.4 km/s) and low vertical velocity gradients (<~1 s^{-1}) correlate with extrusive volcanics and hummocky morphology, primarily in the fossil hanging wall and volcanic fields. Intermediate shallow velocities (3.4–4.2 km/s) and intermediate-velocity gradients (1–3 s^{-1}) correlate with massive outcrops of serpentinized peridotite, dominating the central (Abel Dome and western half of Cain Dome) and southeastern parts of the OCC. High velocities near the seafloor (>4.2 km/s) and large-velocity gradients (>3 s^{-1}) are

interpreted as large gabbro plutons and are mostly present beneath the Babel Dome and eastern half of the Cain Dome (Xu et al., 2009) (Figure 1b).

3. Early-Arrival FWI

After preprocessing (Text S1), we applied acoustic early-arrival FWI to the MCS data (Text S2). FWI models are derived by fully exploiting kinematic and dynamic information from early arrival seismic refraction data (Figures S1 and S2 of the supporting information). Our FWI runs were performed from low to high frequency in two main steps: 6-8-10-15 and 6-8-15-20 Hz. The starting velocity models were the traveltime tomography models of Xu et al. (2009). The influence of unrealistically high velocities of the starting models below ~2-km depth was assessed through an FWI test with a modified starting model in which all velocity values larger than 7.0 km/s are set to 7.0 km/s for Profile K1, and the test gives us confidence that our results in the upper ~2 km are robust and not significantly influenced by the unconstrained velocities >2 km below seafloor in the starting models (Figure S7). Ricker source wavelets with central frequency of 5 and 8 Hz (Figure S3a) were used for the two-step runs, respectively. The model updates occur not only in the shallow part but also deeper than the first-arrival ray coverage predicted by the traveltime tomography models (Figure 2). The validity of the final velocity models can be qualitatively assessed by comparing the observed traces with synthetic traces predicted by the traveltime tomography and the final FWI velocity models. Although could not fit all the later wiggles, the waveform inversion has been able to fit a significant part of the data, showing a clear improvement in the match between observed and predicted early-arrival refractions (Figure S6). Checkerboard resolution tests indicate that FWI models can resolve features as small as 0.5 km by 0.5 km (Figure S8h) for most of the models' domain, except at the ends of profiles where data coverage and resolution are poor. In some shallow regions best sampled by the data, features with thicknesses of ~0.25 km are resolvable (Figures S8i and S8j). In addition, despite the small drop in misfit function obtained during the inversions (Figure S9) and the nonuniqueness of the inversions, the large-scale similarity and clear improvement in the small-scale structures (Figure S10) and deeper illumination of the FWI models (Figure 2) with respect to traveltime tomography models indicate that the final models are realistic, and provide confidence when interpreting them.

The large lateral velocity variations (Figure 3) in both strike and dip directions can be seen clearly by displaying the FWI models relative to a 1-D reference model (Figure S3b). The most striking feature of the FWI models are the high-velocity bodies beneath the detachment surface at the Cain Dome (the central sections of Dip Profiles K1, K4, and K8, and the northern two thirds of Strike Profile K7), and at the southern end of K5 (Figures 2 and 3). These high-velocity anomalies are embedded within a more intermediate background velocity, which is prevalent near the terminations and western flank of Cain Dome and beneath the Abel and the Eve Domes. Low-velocity zones are present primarily in the hanging wall at the eastern ends of the Dip Profiles K4, K1, and K8 and coincident with the seafloor volcanic fields, for example, in the northern and southern parts of K6, and the western end of K8. There is also a small patch of low velocities located at the western end of K1.

4. RTM

The RTM images were derived from migrating preprocessed MCS shot gathers (Figure S11) based on high-fidelity FWI models (Figure 2) to investigate the structural variability within the Kane OCC (Text S3). To aid interpretation, RTM images (Figure S12) are shown together with *P* wave velocity variations (relative to a 1-D structure with seafloor velocity of 3.7 km/s and vertical velocity gradient of 1.75 s^{-1}, Figure S3b) to highlight the correlation between velocity variations and the RTM imaged features. The RTM images reveal a geometrically complex reflection image underlying the OCC domes and extending to across the eastern hanging wall and volcanic fields, showing distinct reflectivity patterns in shallow lithosphere compared to normal crust (Figure 3).

Consistent with velocity variations, RTM images show evidence for the heterogeneous structure of the upper lithosphere at Kane OCC, with more reflective and chaotic image sections correlated to the low-velocity zones. The low reflectivity and/or seismically transparent sections are present beneath easternmost Cain Dome along the Dip Profiles K4 and K1, the Profiles K8, K5, and K6, and at the northern two thirds of K7. The higher and more chaotic reflectivity, and in some cases with layered reflectors, subparallel to the

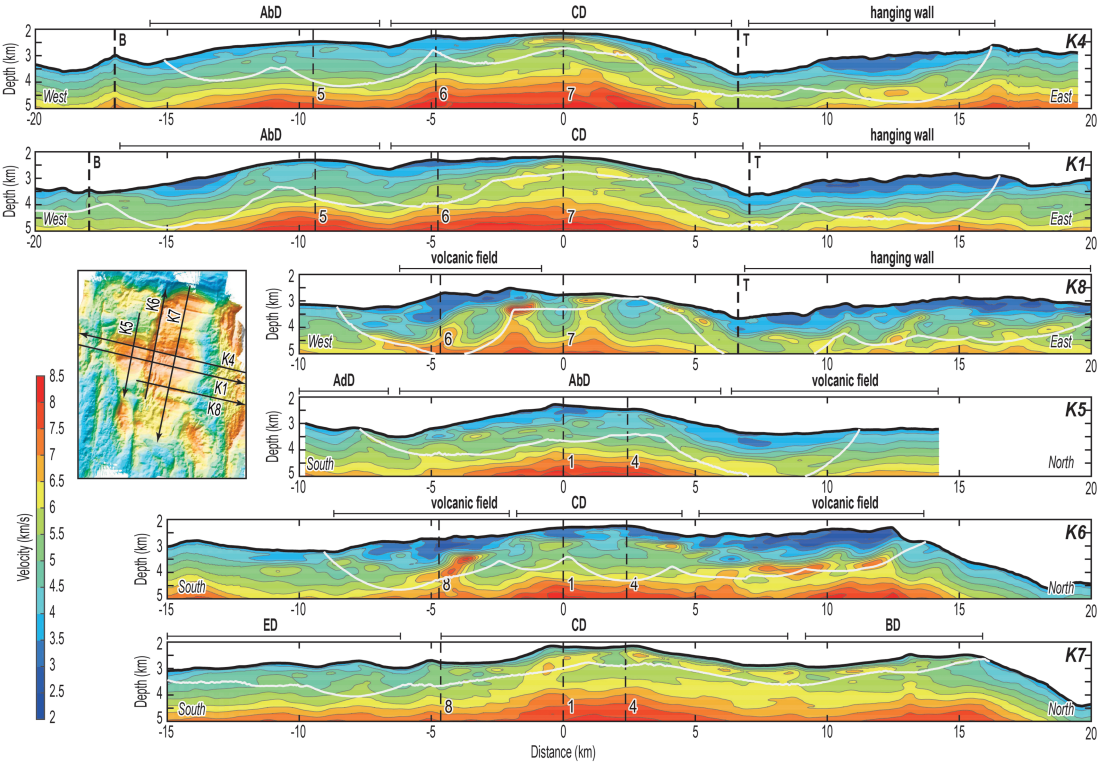

Figure 2. Two-dimensional full waveform inversion models of *P* wave velocity beneath Kane OCC. Contour interval is 0.5 km/s. Profile locations are shown in the inset. Morphological features are labeled at the top of the profiles. Thick dashed lines indicate locations of breakaway (B) and termination (T). Thin dashed lines show crossings between dip and strike profiles. The limit of the ray coverage for the traveltime tomography inversion is indicated by a solid white line. Models are shown with no vertical exaggeration.

seafloor are mostly present in the hanging wall and underneath the interpreted volcanic fields. The transition from transparent domes to chaotic hanging wall is abrupt, as seen near the termination along Profiles K1 and K4. In some cases the chaotic reflectivity overlaps a more seismically transparent section, as found along K6 and the western flank of the Cain Dome along Profiles K1 and K4.

5. Discussion

The lithospheric structure exhumed by ODFs is far from the standard ophiolite-based Penrose model. The geological interpretation of the traveltime tomography models is basically based on in situ geological samples and seafloor morphology at Kane and Atlantis Massif OCCs, and dominant gabbro recovered from the 1.4-km-deep IODP Hole U1309D drilled on the ODF of the Atlantis Massif (Blackman et al., 2011). Our new FWI models (Figure 2) and RTM images (Figure 3) illuminate in great detail the lateral structural heterogeneity up to ~2 km beneath the Kane OCC, providing an opportunity to discuss the thickness of the volcanic units, size, and thickness of the gabbroic bodies across the domes and to use this information to quantify magmatism during OCC evolution. Based on the velocity structures, velocity variations, and reflection images, we identify four lithological domain features (Figure 4) in our RTM images: basalt, gabbro, serpentinized mantle, and less altered mantle and/or mantle with variable amounts of gabbro.

5.1. Thickness of the Volcanic Units

FWI models show that low-velocity zones are systemically correlated with pillow basalts on top of volcanic fields that formed along the East Fault, and volcanic terrain with hummocky morphology in the hanging wall (Figure 2). RTM images of these low-velocity zones show a more reflective and chaotic section typical of slow-spreading upper magmatic crust (e.g., Mutter & Karson, 1992) (Figure 3). We thus interpret these low-velocity zones as dominantly extrusive volcanics, with a mixture of an uncertain proportion of

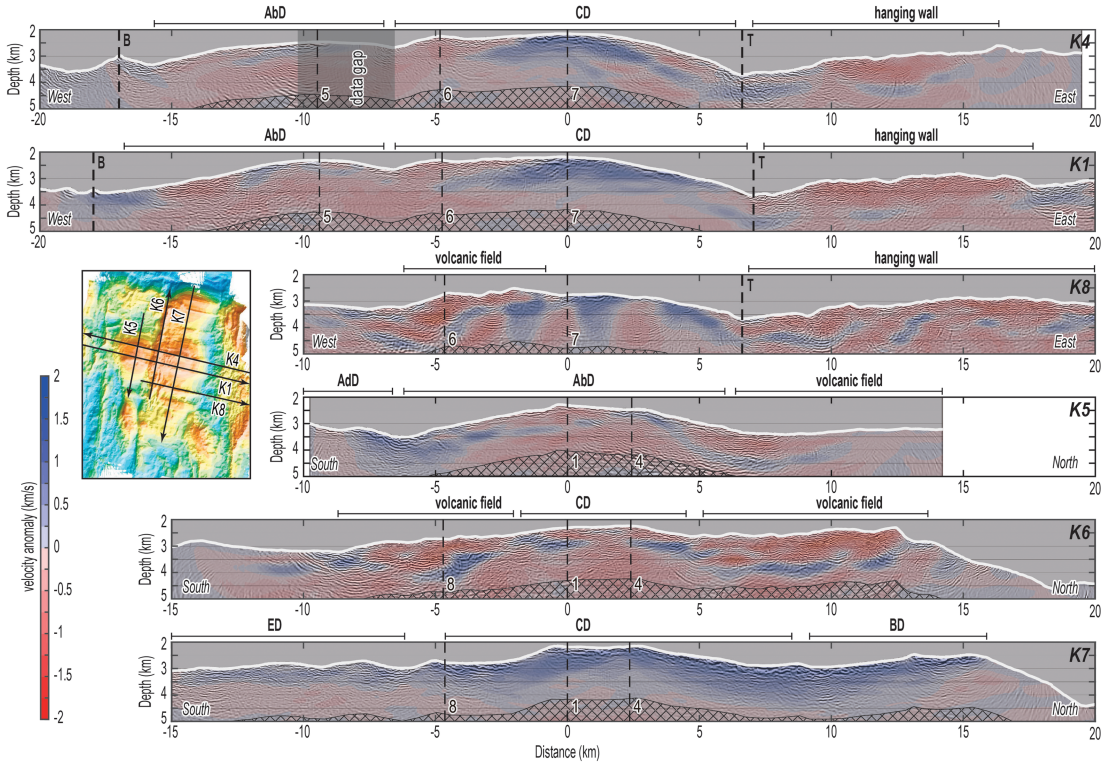

Figure 3. RTM images overlain on velocity variations relative to a 1-D model (Figure S3b). The shaded area indicates data gap of MCS acquisition of Profile K4. Models and images are shown with no vertical exaggeration. Profile locations are indicated in the left inset. The stippled regions were excluded from interpretation.

underlying sheeted dikes (Figure 4). The basaltic sections are present along the western part of Profile K8, both ends of Profile K6, the western part of Profile K1, northern part of Profile K5, and the eastern end of dip profiles in the hanging wall.

Beneath the southern volcanic field, the basaltic layer has a maximum thickness of 1.7 km, protruding downward at the center (at −5-km model distance of Profiles K8 and K6), with a total estimated volume of at least 64 km^3. Beneath the northern Mt. Ararat volcanic field, the basaltic layer has a more uniform thickness of ~1.2 km toward the northern transform wall, and extends shallowly beneath the northwestern section of Cain Dome (K6) and northern section of Abel Dome (K5). The basaltic layer at the eastern ends of the dip profiles in the hanging wall has an average thickness of ~1.0 km and extends further west toward the elevated domes from north to south (Figure 4). An ~1-km-thick basaltic layer next to the breakaway is located in the west of Abel Dome along Profile K1 (Figure 3), probably corresponding to the volcanic crust in which the detachment initiated.

5.2. The Shape of the Gabbroic Bodies Across the Domes

New FWI models and RTM images illuminate in great detail the shape of the larger gabbroic bodies beneath Cain and Babel Domes and show evidence for smaller gabbroic units beneath the other domes (Figure 4). The interpreted gabbroic bodies show a bimodal distribution in terms of size and location within the Kane OCC. Large gabbroic bodies are observed beneath the Cain Dome along Profiles K4, K1, and K7 and also shown beneath the Babel Dome along Profile K7. Lithological variations from the breakaway to termination along Dip Profiles K4 and K1 across the Cain Dome are very similar (Figure 4). A large elongated gabbroic body with an average thickness of ~600 m is located beneath the central and eastern sections of Cain Dome along Profiles K4 and K1. The size in the dip direction of this large gabbroic body as measured along profiles K4 and K1 is ~5.5 and 10 km, respectively. The large gabbroic body beneath the Cain Dome extends continuously to the north beneath the Babel Dome with a maximum thickness of ~1.0 km as imaged along

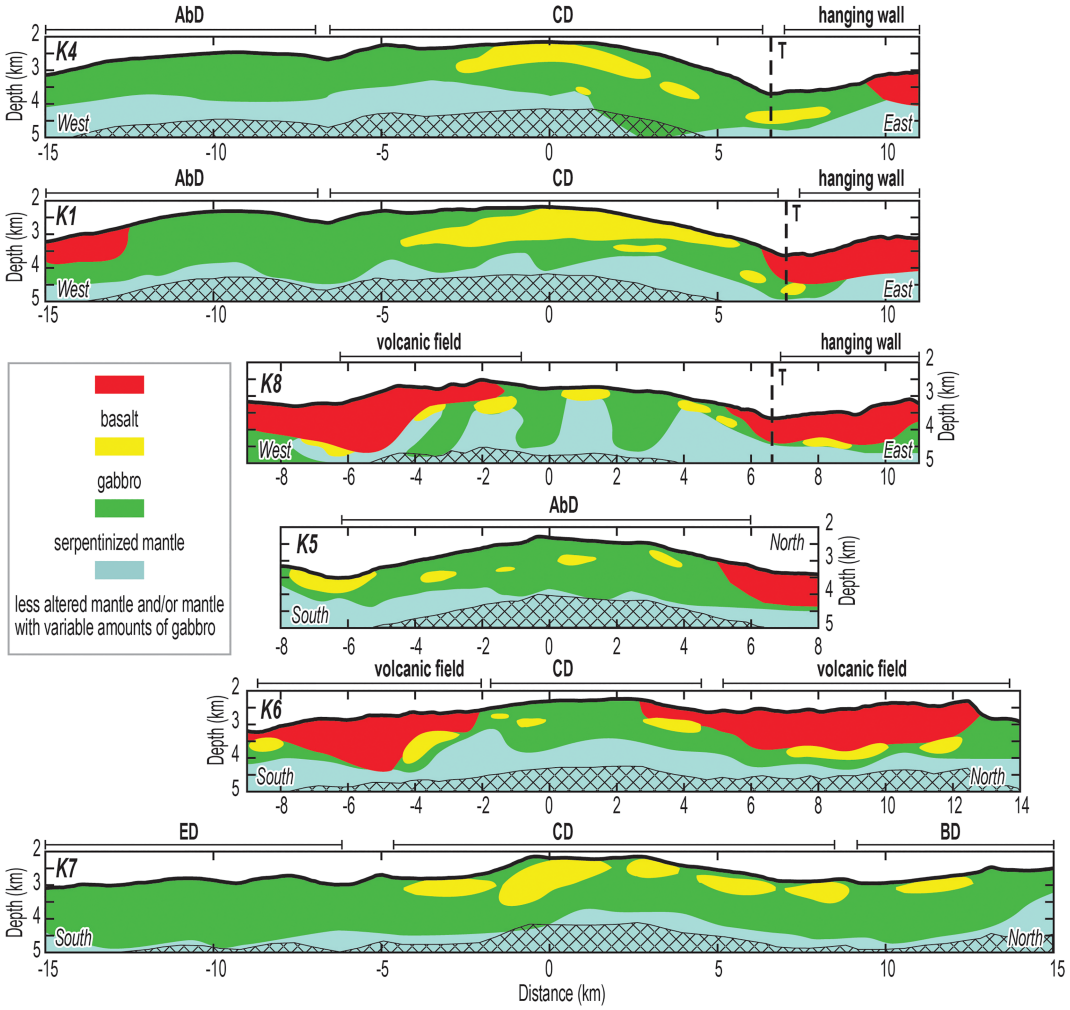

Figure 4. Lithological structure interpretations along the seismic profiles. Images are shown with no vertical exaggeration.

Profile K7. It is shown as several discrete gabbroic bodies next to each other and has a total along-strike length of ~17 km. To the south, this gabbroic body does not extend into the Eve Dome. It seems to finger southward from the southern flank of Cain Dome, as evidenced by the alternating high- and intermediate-velocity bodies imaged along Profile K8 between the termination and −3-km model distance.

Our new FWI models and RTM images also reveal the presence of several elongated gabbroic bodies of smaller size with length of 0.5–3.0 km and thickness of 200–500 m. Many of these are embedded in a predominately serpentinized peridotite beneath the Abel Dome (K5), western flank of Cain Dome (K6), and eastern flank of the Cain Dome (K4 and K8). Other similarly sized gabbroic bodies are located beneath the volcanic fields and hanging wall (K6 and K8).

Lithological distribution along the strike profiles shows greater variability (Figure 4). A prominent gabbroic body with length of ~2 km and thickness of ~0.5 km exists at the southern section of Profile K5 approaching Adam Dome. Several small isolated gabbroic bodies are decentralized in their distribution with respect to the Abel Dome. Profile K6 crosses the two volcanic fields to the south and north. Gabbroic bodies are found dispersed beneath the interpreted basalt, and two smaller ones are located beneath the southern section of Cain Dome.

The southern section of Profile K7 shows a slighter smaller velocity and not so transparent seismic image compared to the northern section (Figure 3); thus, we interpret that area as predominantly serpentinized mantle although a mixture of gabbro and serpentinized mantle might be the case.

5.3. Magmatism During OCC Evolution

Understanding the origin and distribution of the gabbroic bodies is crucial to determining the formation and evolution processes of OCCs (Ildefonse et al., 2007). The heterogeneous distribution of gabbroic bodies within the Kane OCC (Figure 4) indicates strong spatial and temporal variability in magmatism.

Geological interpretation of Dip Profiles K4 and K1 indicates that mantle was exhumed near the breakaway underneath Abel Dome, suggesting the Kane ODF was formed under a very low magma environment and initially cut through a thin crust. Strike Profile K5, however, shows a strong gabbroic intrusion to the south near the Adam Dome where seafloor gabbroic samples were recovered (Dick et al., 2008). Thus, the ODF reached gabbros at shallow depths, indicating robust magmatism beneath Adam Dome. The small isolated gabbroic bodies imbedded in serpentinized peridotite beneath the Abel Dome shown along Profile K5 can be attributed to a decreasing melt flux to the north, producing smaller, more rapidly crystallized intrusions. Dominantly serpentinized mantle are inferred to be present beneath the western section of the Cain Dome along Profiles K4, K1, and K6, suggesting magma-limited conditions during the exhumation of the central part of Kane OCC, whereas magmatic sections during this period mostly developed at centers beneath the volcanic fields to the south and to the north.

Gabbroic bodies overlaid by volcanic basalts are shown in the western side of Profile K8, and both ends of Profile K6, where irregular, hummocky morphology indicates volcanic fields are present (Dick et al., 2008). The spatial association of the volcanic fields with East Fault suggests that the magma was extruded along the fault during exhumation of the ODF (Dick et al., 2008), caused by the bending-related differential stress (Tucholke et al., 2001).

A significant change in the distribution of gabbroic bodies happens beneath the Babel Dome and central and eastern sections of Cain Dome. The large gabbroic plutons were intruded beneath the ODF, suggesting robust magmatism during the late stage of Kane OCC formation. This gabbroic unit probably represents larger and more frequent intrusions, with a total estimated volume of >80 km^3 beneath the Cain and Babel Domes. This late stage northern magmatism is also evidenced by the more elevated seafloor in the hanging wall adjacent to Babel Dome and Cain Dome than the Eve Dome.

Acknowledgments
Seismic data acquisition was funded by NSF Grant OCE99-87004. Data files can be obtained from Interdisciplinary Earth Data Alliance (IEDA) (https://doi.org/10.1594/IEDA/314508) (Tucholke & Collins, 20142014). The velocity models and migrated seismic sections shown in the paper are freely available for download from 4TU. Centre for Research Data (doi:10.4121/uuid:3ef55160-4a5a-4d1a-b734-fe2b8d2871ae). Full waveform inversion was performed with the software TomoPlus (GeoTomo LLC) licensed to SCSIO. This research was supported by the National Natural Science Foundation of China (41676044 and 91858207) and Special Foundation for National Science and Technology Basic Research Program of China (2018FY100505). M. X. acknowledges supports from Guangdong NSF research team project (2017A030312002), K. C. Wong Education Foundation (GJTD-2018-13), Key Special Project for Introduced Talents Team of Southern Marine Science and Engineering Guangdong Laboratory (GML2019ZD0205), and the Strategic Priority Research Program of the Chinese Academy of Sciences (XDA13010105). J. P. C. acknowledges support from the Independent Research and Development Program at WHOI. J. P. Wang and X. R. Mu from China University of Petroleum are thanked for helping with the RTM setup.

References

Auzende, J.-M., Cannat, M., Gente, P., Henriet, J. P., Juteau, T., Karson, J., et al. (1994). Observation of sections of oceanic crust and mantle cropping out on the southern wall of Kane FZ (N. Atlantic). *Terra Nova*, *6*(2), 143–148. https://doi.org/10.1111/j.1365-3121.1994.tb00647.x

Blackman, D. K., Ildefonse, B., John, B. E., Ohara, Y., Miller, D. J., Abe, N., et al. (2011). Drilling constraints on lithospheric accretion and evolution at Atlantis Massif, Mid-Atlantic Ridge 30°N. *Journal of Geophysical Research*, *116*, B07103. https://doi.org/10.1029/2010JB007931

Blackman, D. K., Karson, J. A., Kelley, D. S., Cann, J. R., Früh-Green, G. L., Gee, J. S., et al. (2002). Geology of the Atlantis Massif (Mid-Atlantic Ridge, 30°N): Implications for the evolution of an ultramafic oceanic core complex. *Marine Geophysical Researches*, *23*(5/6), 443–469. https://doi.org/10.1023/B:MARI.0000018232.14085.75

Buck, W. R., Lavier, L. L., & Poliakov, A. N. B. (2005). Modes of faulting at mid-ocean ridges. *Nature*, *434*(7034), 719–723. https://doi.org/10.1038/nature03358

Canales, J. P. (2010). Small-scale structure of the Kane Oceanic Core Complex, Mid-Atlantic Ridge 23°30′N, from waveform tomography of multichannel seismic data. *Geophysical Research Letters*, *37*, L21305. https://doi.org/10.1029/2010GL044412

Canales, J. P., Tucholke, B. E., Xu, M., Collins, J. A., & Dubois, D. L. (2008). Seismic evidence for large-scale compositional heterogeneity of oceanic core complexes. *Geochemistry, Geophysics, Geosystems*, *9*, Q08002. https://doi.org/10.1029/2008GC002009

Cann, J. R., Blackman, D. K., Smith, D. K., McAllister, E., Janssen, B., Mello, S., et al. (1997). Corrugated slip surfaces formed at ridge-transform intersections on the Mid-Atlantic Ridge. *Nature*, *385*(6614), 329–332. https://doi.org/10.1038/385329a0

Dannowski, A., Grevemeyer, I., Ranero, C. R., Ceuleneer, G., Maia, M., Phipps Morgan, J., & Gente, P. (2010). Seismic structure of an oceanic core complex at the Mid-Atlantic Ridge, 22°19′N. *Journal of Geophysical Research*, *115*, B07106. https://doi.org/10.1029/2009JB006943

Dick, H. J. B., Kvassnes, A. J. S., Robinson, P. T., MacLeod, C. J., & Kinoshita, H. (2019). The Atlantis Bank Gabbro Massif, Southwest Indian Ridge. *Progress in Earth and Planetary Science*, *6*(1), 1–70. https://doi.org/10.1186/s40645-019-0307-9

Dick, H. J. B., Natland, J. H., Alt, J. C., Bach, W., Bideau, D., Gee, J. S., et al. (2000). A long in situ section of the lower ocean crust: Results of ODP Leg 176 drilling at the Southwest Indian ridge. *Earth and Planetary Science Letters*, *179*(1), 31–51. https://doi.org/10.1016/s0012-821x(00)00102-3

Dick, H. J. B., Tivey, M. A., & Tucholke, B. E. (2008). Plutonic foundation of a slow-spread ridge segment: Oceanic core complex at Kane Megamullion, 23°30′N, 45°20′W. *Geochemistry, Geophysics, Geosystems*, *9*, Q05014. https://doi.org/10.1029/2007GC001645

Escartín, J., & Canales, J. P. (2011). Detachments in oceanic lithosphere: Deformation, magmatism, fluid flow and ecosystems. AGU Chapman Conference on Oceanic Detachments. Agros, Cyprus, 8–15 May 2010. *Eos, Transactions, American Geophysical Union*, *92*(4), 31. https://doi.org/10.1029/2011EO040003

Escartín, J., Mével, C., MacLeod, C. J., & McCaig, A. M. (2003). Constraints on deformation conditions and the origin of oceanic detachments: The Mid-Atlantic Ridge core complex at 15°45′N. *Geochemistry, Geophysics, Geosystems*, *4*(8), 1067. https://doi.org/10.1029/2002GC000472

Escartín, J., Mével, C., Petersen, S., Bonnemains, D., Cannat, M., Andreani, M., et al. (2017). Tectonic structure, evolution, and the nature of oceanic core complexes and their detachment fault zones (13°20′N and 13°30′N, Mid Atlantic Ridge). *Geochemistry, Geophysics, Geosystems*, *18*, 1451–1482. https://doi.org/10.1002/2016GC006775

Grimes, C. B., Cheadle, M. J., John, B. E., Reiners, P. W., & Wooden, J. L. (2011). Cooling rates and the depth of detachment faulting at oceanic core complexes: Evidence from zircon Pb/U and (U-Th)/He ages. *Geochemistry, Geophysics, Geosystems*, *12*, Q0AG01. https://doi.org/10.1029/2010GC003391

Harding, A. J., Arnulf, A. F., & Blackman, D. K. (2016). Velocity structure near IODP Hole U1309D, Atlantis Massif, from waveform inversion of streamer data and borehole measurements. *Geochemistry, Geophysics, Geosystems*, *17*, 1990–2014. https://doi.org/10.1002/2016GC006312

Harding, J. L., van Avendonk, H. J. A., Hayman, N. W., Grevemeyer, I., Peirce, C., & Dannowski, A. (2017). Magmatic-tectonic conditions for hydrothermal venting on an ultraslow-spread oceanic core complex. *Geology*, *45*(9), 839–842. https://doi.org/10.1130/G39045.1

Henig, A. S., Blackman, D. K., Harding, A. J., Canales, J. P., & Kent, G. M. (2012). Downward continued multi-channel seismic refraction analysis of Atlantis Massif oceanic core complex, 30°N Mid-Atlantic Ridge. *Geochemistry, Geophysics, Geosystems*, *13*, Q0AG07. https://doi.org/10.1029/2012GC004059

Ildefonse, B., Blackman, D. K., John, B. E., Ohara, Y., Miller, D. J., MacLeod, C. J., & Party, I. O. E. S. (2007). Oceanic core complexes and crustal accretion at slow-spreading ridges. *Geology*, *35*(7), 623–626. https://doi.org/10.1130/G23531A.1

MacLeod, C. J., Searle, R. C., Murton, B. J., Casey, J. F., Mallows, C., Unsworth, S. C., et al. (2009). Life cycle of oceanic core complexes. *Earth and Planetary Science Letters*, *287*(3–4), 333–344. https://doi.org/10.1016/j.epsl.2009.08.016

Mutter, J. C., & Karson, J. A. (1992). Structural processes at slow-spreading ridges. *Science*, *257*(5070), 627–634. https://doi.org/10.1126/science.257.5070.627

Olive, J.-A., Behn, M. D., & Tucholke, B. E. (2010). The structure of oceanic core complexes controlled by the depth distribution of magma emplacement. *Nature Geoscience*, *3*(7), 491–495. https://doi.org/10.1038/ngeo888

Parnell-Turner, R., Sohn, R. A., Peirce, C., Reston, T. J., MacLeod, C. J., Searle, R. C., & Sima, N. M. (2017). Oceanic detachment faults generate compression in extension. *Geology*, *45*(10), 923–926. https://doi.org/10.1130/G39232.1

Planert, L., Flueh, E. R., Tilmann, F., Grevemeyer, I., & Reston, T. (2010). Crustal structure of a rifted oceanic core complex and its conjugate side at the MAR at 5°S: Implications for melt extraction during detachment faulting and core complex formation. *Geophysical Journal International*, *181*(1), 113–126. https://doi.org/10.1111/j.1365-246X.2010.04504.x

Tucholke, B. E., Behn, M. D., Buck, R., & Lin, J. (2008). The role of melt supply in oceanic detachment faulting and formation of megamullions. *Geology*, *36*(6), 455–458. https://doi.org/10.1130/G24639A.1

Tucholke, B. E., & Collins, J. A. (2014). Raw multi-channel seismic shot data from the northern Mid-Atlantic Ridge acquired during R/V Maurice Ewing expedition EW0102 (2001). Interdisciplinary earth data Alliance (IEDA), doi:https://doi.org/10.1594/IEDA/314508.

Tucholke, B. E., Fujioka, K., Ishitara, T., Hirth, G., & Kinoshita, M. (2001). Submersible study of an oceanic megamullion in the central North Atlantic. *Journal of Geophysical Research*, *106*(B8), 16,145–16,161. https://doi.org/10.1029/2001JB000373

Tucholke, B. E., Lin, J., & Kleinrock, M. C. (1998). Megamullions and mullion structure defining oceanic metamorphic core complexes on the Mid-Atlantic ridge. *Journal of Geophysical Research*, *103*(B5), 9857–9866. https://doi.org/10.1029/98jb00167

Williams, C. M. (2007). Oceanic lithosphere magnetization: Marine magnetic investigations of crustal accretion and tectonic processes in mid-ocean ridge environments, (Doctoral dissertation). Retreved from Mass. Inst. of Technol., Woods Hole Oceanogr. Inst., Woods Hole, Mass. https://doi.org/10.1575/1912/2031.

Xu, M., Canales, J. P., Tucholke, B. E., & Dubois, D. L. (2009). Heterogeneous seismic velocity structure of the upper lithosphere at Kane oceanic core complex, Mid-Atlantic Ridge. *Geochemistry, Geophysics, Geosystems*, *10*, Q10001. https://doi.org/10.1029/2009GC002586